

# Slow neutron production as a probe of nuclear transparency and hadron formation in high-energy $\gamma^*A$ reactions

A.B. Larionov<sup>1,2,3a</sup>, M. Strikman<sup>4b</sup>

<sup>1</sup>*Frankfurt Institute for Advanced Studies (FIAS),*

*D-60438 Frankfurt am Main, Germany*

<sup>2</sup>*National Research Center "Kurchatov Institute", 123182 Moscow, Russia*

<sup>3</sup>*Institut für Kernphysik, Forschungszentrum Jülich, D-52425 Jülich, Germany*

<sup>4</sup>*Pennsylvania State University, University Park, PA 16802, USA*

(Dated: January 11, 2019)

## Abstract

Studies of the hadron formation in hard processes on nuclei were focusing on hadrons in the current fragmentation region. Little is known about the space-time picture of formation of hadrons in the nucleus fragmentation region, in particular, in deep inelastic scattering (DIS). Study of the nucleus decay via emission of neutrons provides a rare opportunity to probe this domain at collider energies. This paper reports on the hybrid dynamical+statistical (GiBUU+SMM) calculations of neutron production in proton-, muon- and virtual photon-induced collisions with nuclei. We confirm the conclusion that the E665 data on neutron production in  $\mu^- + \text{Pb}$  DIS indicate a strong suppression of the final state interaction for hadrons with momenta above a value as low as  $\sim 1$  GeV/c. This is well below the momentum range for which formation time and color transparency effects become important. In a short-run perspective, the ultraperipheral heavy-ion collisions at the LHC and RHIC can be used to test this suppression. We focus on the direct photon process in which a photon coherently emitted by one nucleus interacts with a gluon from another nucleus producing a pair of jets. We present our predictions for the neutron multiplicity distributions and  $p_t$ -spectra in photon - nucleus collisions at the energies accessible at the LHC and RHIC for direct photon kinematics for several models of hadron formation. We argue that ultimately studies of the neutron production in  $\gamma A$  collisions would open a new window on the small  $x$  dynamics and hadron component of the photon wave function.

---

<sup>a</sup> E-mail address: larionov@fias.uni-frankfurt.de

<sup>b</sup> E-mail address: mxs43@psu.edu

## 1. INTRODUCTION

Understanding the dynamics of a high-energy particle-nucleus interaction based on first-principle QCD is still a challenge. One is usually forced to use phenomenological approaches. There are several questions which naturally arise:

- How to match partonic and hadronic degrees of freedom?
- To what extent are the nuclear modifications important, i.e. the production cross sections deviate from the linear  $A$ -dependence due to absorption and/or due to nuclear parton distribution functions ?
- How do the secondary particles interact with the nucleus: as ordinary hadrons or as transient quark - gluon configurations (“prehadrons”) ?

The elementary hadron-nucleon interactions may be modified inside nucleus since the quark - gluon wave packages which in the end would evolve into fast hadrons are not yet formed during a short time they pass through the nucleus.

It is expected that the partonic configurations involved in an exclusive hard lepton- or hadron-nucleon scattering process have a reduced transverse size at the hard interaction point. The interaction strength of such compact configurations with nucleons of the nucleus is therefore reduced. This is known as a color transparency (CT) phenomenon (see reviews [1–3]). Though hadrons,  $h$  interact in compact configurations close to the hard interaction point, they expand to the average-size configurations at the coherence length distance

$$l_c = 2P/\Delta M_h^2 \sim 0.4 \div 0.6(fm/GeV) \cdot p[GeV], \quad (1)$$

where  $p$  is the momentum of expanding configuration. The CT effects get stronger with growing momentum  $p$  and ultimately lead to an almost complete disappearance of the initial and final state hadronic interactions when the coherence length is much larger than the nuclear size. The CT has been observed in high-energy experiments, such as pion dissociation into two jets at Fermilab [4], photoproduction of  $J/\psi$  at Fermilab [5], muon-induced exclusive  $\rho^0$  production at Fermilab [6], and exclusive vector meson production at HERA [7, 8]. All these experiments were focusing on the fast particle production in hard interactions.

Another interesting possibility to study the formation of hadrons has been suggested in the E665 experiment at Fermilab [9] where the slow ( $E < 10$  MeV) neutrons in 470 GeV

muon DIS off nuclear targets have been detected. As one emitted neutron carries off about 10 MeV of the nuclear excitation energy, counting slow neutrons allows to use the nucleus as a “micro calorimeter” for the particles produced in the DIS process. More transparent is the nucleus for the energetic products – fewer slow neutrons will be emitted. This correlation allows to put limits on the hadron formation length

$$l_h = \frac{2p_h}{\Delta M^2} \quad (2)$$

by using the nuclear transport models.

The coherence length  $l_c$  for the expansion of a small configuration and the formation length  $l_h$  traveled by a parton before it transforms into a system of incoherently interacting hadrons are, in principle, different (although duality arguments suggest that they should be similar). These lengths may also depend on the hadron  $h$  and on the hard probe, namely whether the hard process involves the removal of a quark or a gluon from the nucleus.

The growth of the formation length with the struck parton energy explains the experimental observation that at large hadron momenta corresponding to  $l_h \gg 2R_A$  the spectra of hadrons in the current fragmentation region off heavy and light nuclei practically coincide. Moreover, in the transitional energy range where the formation length is comparable to the nucleus size, the rate of absorption of the leading hadrons is well described by the model with the rate of expansion similar to one used for description of the CT phenomena, see ref. [10] and discussion below.

It is expected from the analyses of pion electroproduction at TJNAF [11, 12], that  $\Delta M^2 \simeq 0.7 \text{ GeV}^2$ . Thus, Eq.(2) suggests that only slow enough particles, with momenta less than, say, several GeV/c, will be formed inside nucleus and experience secondary interactions with target nucleons. This picture is qualitatively supported by the first theoretical analysis [13] of the data [9] which demonstrated that for the description of the data one has to assume that only nucleons produced in the elementary reaction with typical momenta  $\leq 1 \text{ GeV}/c$  may interact in the nucleus. However, this is an amazingly low cutoff as according to Eq.(2) hadrons with momenta  $\leq 10 \text{ GeV}/c$  are typically formed inside the lead nucleus.

In this work we study the slow neutron production in quasi-real photon interactions of TeV energies with nuclear target. Such interactions can be studied in ultraperipheral heavy-ion collisions (UPC) at RHIC and LHC. We focus on the sensitivity of the slow neutron production to the interaction strength of energetic particles with nucleons. The

calculations are based on the Giessen Boltzmann-Uehling-Uhlenbeck (GiBUU) model [14] and the statistical multifragmentation model (SMM) [15, 16].

The paper is structured as follows. In sec. 2 we briefly describe the theoretical framework which includes the  $\gamma^*N$  event simulation by PYTHIA model (which is a part of the GiBUU package), the propagation of produced particles through the nucleus which leads to the energy deposition in the form of hole excitations in the nuclear residue, and the statistical deexcitation of the nuclear residue. Sec. 3 contains numerical results. First, we benchmark the model against experimental data on slow neutron production in  $pA$  collisions at  $p_{\text{lab}} \sim 1$  GeV/c and in  $\mu^- + A$  collisions at 470 GeV. Next we perform calculations for the LHC and RHIC kinematics of heavy-ion collisions in which one of the nuclei serves as a source of quasireal photons. We focus on the simplest direct photon kinematics in which a photon interacts with a gluon of the nucleus producing two back-to-back jets (i.e. jets with balancing transverse momenta carrying most of the photon longitudinal momentum):  $\gamma g \rightarrow q\bar{q}$ . We show that the energy spectrum and the multiplicity of soft neutrons is directly related to pre-hadronic interactions in the nucleus. In sec. 4 we discuss the directions for further studies, in particular, the expectations for neutron production in the resolved photon kinematics. Sec. 5 contains the summary of our results and conclusions.

## 2. THEORETICAL FRAMEWORK

In our analysis we will use the GiBUU model [14]. It solves the coupled set of kinetic equations for the system of hadrons explicitly in time and space. Between collisions and resonance decays the particles propagate according to the Hamiltonian equations of motion with the mean field potentials. The nuclear potential is described within the relativistic mean field model NL3 of ref. [17]. The Coulomb potential acting on charge particles is also included. Particle collisions are simulated within the geometrical minimum distance scheme. The two particles which are passing their minimal distance  $d$  during the given time step will collide during this time step if  $d < \sqrt{\sigma_{\text{tot}}/\pi}$  where  $\sigma_{\text{tot}}$  is the total interaction cross section of these particles. Collisions are simulated by a Monte-Carlo algorithm taking into account elastic and inelastic scattering channels. If the invariant energy  $\sqrt{s}$  is larger than some threshold value (2.2 GeV for meson-baryon collision, 3.4 GeV for baryon-baryon collision, and 2.38 GeV for antibaryon-baryon collision), the hadron-hadron collision is simulated via

PYTHIA version 6.4 [18] and (for antibaryon-baryon collisions only) FRITIOF version 7.02 [19] models. The proton and neutron density profiles are chosen in the Woods-Saxon form with geometrical parameters taken from the Skyrme-Hartree-Fock systematics [20]. The Fermi motion is taken into account in the local Fermi approximation. The Pauli blocking factors are included for the nucleons in the final state of scattering events. The nuclear mean field and Pauli blocking factors are supposed to be constant during the time evolution of the hadronic system. This allows to save CPU time for the elementary-particle-induced reactions on nuclei without significant accuracy lost.

There is also one important technical aspect which deserves to be mentioned. Most of the previous GiBUU calculations for the lepton-nucleus interactions were done with the so-called perturbative particles to increase statistics and save CPU time, see e.g. Appendix D.2 of ref. [14]. This method works very well for fast particles but not for slow ones, since the nucleus stays intact in calculations with perturbative particles. In particular, using perturbative particles would lead to the drastic overestimation of the number of holes in the nucleus, see discussion below in this section. Therefore, to avoid such problems, we apply in calculations the real-particles method which takes into account the trailing of the nucleus in the course of the cascade and thus provides much better description of the energy deposition in the nuclear residue.

In the case of high energy lepton-nucleus interaction the struck nucleon is chosen randomly neglecting nuclear shadowing effects, see discussions below in secs. 3.2 and 3.3. This corresponds to the probability distribution of the interaction with protons and neutrons

$$dP_i = \frac{\rho_i(\mathbf{r})d^3r}{A}, \quad i = p, n. \quad (3)$$

The collision of virtual photon with the struck nucleon is simulated via PYTHIA.

The kinematics of the lepton scattering depends on experimental conditions. In the case of DIS the elementary lepton-nucleon cross section can be written as follows (cf. [21]):

$$\frac{d\sigma}{d\Omega dE'} = \Gamma[\sigma_T(W^2, Q^2) + \epsilon\sigma_L(W^2, Q^2)], \quad (4)$$

where  $\Omega$  and  $E'$  are, respectively, the solid angle and the energy of the scattered lepton in the laboratory frame,

$$\Gamma = \frac{\alpha E'(W^2 - m_N^2)}{(2\pi)^2 Q^2 m_N E(1 - \epsilon)} \quad (5)$$

is the flux of virtual photons,  $\sigma_T(\sigma_L)$  is the photoabsorption cross section for purely transverse (longitudinal) photons, and

$$\begin{aligned} \epsilon &= \left[ 1 + 2\left(1 + \frac{\nu^2}{Q^2}\right) \tan^2 \frac{\theta}{2} \right]^{-1} \\ &= \frac{2(1 - y - Q^2/4E^2)}{2(1 - y - Q^2/4E^2) + y^2(1 + Q^2/\nu^2)} \end{aligned} \quad (6)$$

is the relative flux of longitudinal virtual photons,  $y = \nu/E$  is the fraction of the beam energy  $E$  carried off by a virtual photon. The second equality of Eq.(6), which is actually implemented in GiBUU, is satisfied in the limit of the zero lepton mass exactly.

In actual simulations, Eq.(4) has been applied in the rest frame of the struck nucleon (which has a finite momentum due to the Fermi motion) by using the relation

$$\frac{d\sigma}{dydQ^2} = \frac{\pi}{E'} \frac{d\sigma}{d\Omega dE'} \quad , \quad (7)$$

where, in the Lorentz-invariant form,  $y = pq/pk$  with  $p, k$ , and  $q$  being the four-momenta of the struck nucleon, initial lepton, and the virtual photon, respectively. Note that in the present GiBUU calculations the reduced cross section  $\sigma^* = \sigma_T + \epsilon\sigma_L$  is extracted from PYTHIA with default settings (MSTP(14)=30), i.e. it includes the mixture of all possible processes (point-like photon, VMD etc.).

To describe the hadron formation effects we applied the three different prescriptions:

(i) Default formation procedure of the GiBUU model [10, 14, 22] based on the production and formation space-time points extracted from the JETSET part of the PYTHIA. The ratio of the effective prehadron-nucleon cross section  $\sigma_{\text{eff}}$  to the usual total hadron-nucleon cross section  $\sigma_0$  varies linearly with time between production and formation times as

$$\sigma_{\text{eff}}(t)/\sigma_0 = X_0 + (1 - X_0) \frac{t - t_{\text{prod}}}{t_{\text{form}} - t_{\text{prod}}} \quad , \quad (8)$$

where  $X_0 = r_{\text{lead}}a/Q^2$  is the pedestal value of the ratio,  $r_{\text{lead}}$  is the ratio of the number of leading quarks to the total number of quarks in a hadron, and  $a = 1 \text{ GeV}^2$  is a constant factor.

(ii) Quantum diffusion model (QDM) of ref. [23]. In this case the expression for the effective cross section is formally the same as Eq.(8). However, the production time  $t_{\text{prod}}$  is set to the time when the hard interaction happens, while the formation time is defined as  $t_{\text{form}} = t_{\text{prod}} + l_h/c$ . This model has been applied for exclusive hard processes where, in

the interaction point, the hadrons are in small-size configurations. The arguments based on the decomposition of these configurations in a set of hadronic states suggest that for a hadron  $h$   $\Delta M^2 = m_{h^*}^2 - m_h^2$  where  $h^*$  is an excited state of  $h$ . The similar arguments applied for the decomposition of quark wave function suggest that  $\Delta M^2$  should be similar in two cases. The size in the DIS interaction point is more difficult to match to other observations. Since the model has a tendency to overestimate the neutron rate pretty significantly we will make a simplifying assumption that the interaction in the production point is strongly suppressed, that is  $X_0 = 0$ . As we will see below, even with this assumption the model predicts a significantly higher neutron rate than observed experimentally.

(iii) A simple cutoff

$$\sigma_{\text{eff}}/\sigma_0 = \Theta(p_{\text{cut}} - p) , \quad (9)$$

where  $\Theta(x)$  is a Heaviside step function ( $\Theta(x) = 0$  for  $x < 0$  and  $\Theta(x) = 1$  for  $x > 0$ ). The cutoff momentum  $p_{\text{cut}}$  should be of the order of few GeV/c. It can be chosen from comparison with experimental data.

The hadrons produced by the DIS event on the bound nucleon propagate through the nucleus and induce the cascade of interactions which eventually leads to the production of slow neutrons. The latter can be produced either directly or by statistical decay of the excited residual nucleus. The mass number  $A_{\text{res}}$ , charge number  $Z_{\text{res}}$ , excitation energy  $E_{\text{res}}^*$ , and momentum  $\mathbf{p}_{\text{res}}$  of the residual nucleus have been determined in every parallel ensemble<sup>1</sup> by counting the hole excitations as

$$A_{\text{res}} = A - n_{\text{h}} , \quad (10)$$

$$Z_{\text{res}} = Z - \sum_{i=1}^{n_{\text{h}}} Q_i , \quad (11)$$

$$E_{\text{res}}^* = \sum_{i=1}^{n_{\text{h}}} (E_{F,i} - E_i) , \quad (12)$$

$$\mathbf{p}_{\text{res}} = - \sum_{i=1}^{n_{\text{h}}} \mathbf{p}_i , \quad (13)$$

where  $A(Z)$  is the target nucleus mass (charge) number;  $n_{\text{h}}$  is the total number of holes;  $Q_i = 1(0)$  for the proton (neutron) hole;  $E_i$  and  $\mathbf{p}_i$  are, respectively, the single particle energy and momentum;  $E_{F,i}$  is the Fermi energy. The dependence of the Fermi energy on the hole

---

<sup>1</sup> Parallel ensembles can be regarded as “events” in GiBUU simulations.

index “i” is mostly due to the difference of the Fermi energies for protons and neutrons<sup>2</sup>. The hole is added to the nuclear residue every time when the target nucleon is first time involved in some collision process, starting from the initial DIS event. The GiBUU calculation has been stopped at the time  $t = 100$  fm/c (if not mentioned specifically). The directly emitted particles have been determined by requirement of their separation in position space by at least 3 fm from every other particle. The decay of excited nuclear residues has been described with a help of the SMM model.

The SMM model [15, 16] is focused on the description of the multiple simultaneous breakup of the highly-excited nuclear systems (with excitation energy of the order of few MeV/nucleon). But it also includes the sequential decays of the excited fragments which are treated similar to the Weisskopf model [25]. However, in contrast to the Weisskopf model, SMM model includes also the decay width of an excited compound nucleus with respect to the emission of fragments heavier than  $\alpha$ -particle taking into account that the emitted fragment may be in an excited state stable to nucleon emission (see Eq. (34) in ref. [15]). We have applied the SMM model in the evaporation mode, switching-off the simultaneous multifragment breakup, since in the considered reactions the yield of nuclear residues with excitation energies exceeding 1 – 2 MeV per nucleon is small (cf. Fig. 2 below).

### 3. RESULTS

#### 3.1. $pA$ collisions at 1-2 GeV/c

In this intermediate energy range, the effects of hadron formation are unimportant. The proton-nucleus reaction proceeds as a cascade of elastic and inelastic (mainly,  $\Delta$ -resonance production and decay) processes and pion production and reabsorption. The late stage of the reaction, when the fast cascade particles have left the nucleus and the slow deexcitation of the nuclear residue starts – should be, however, similar to the reactions at high energies.

Fig. 1a,b show the neutron energy spectra at the laboratory angle  $120^\circ$  for proton-lead collisions at 1.4 and 2 GeV/c. The proton was initialized at the distance of 0.5 fm from

<sup>2</sup> Since we use the empirical Woods-Saxon density profiles in combination with relativistic mean field potentials, the Fermi energies of protons and neutrons have also some spurious coordinate dependence. Comparison with the calculation using the relativistic Thomas-Fermi method for the nuclear ground states [24] shows, however, that the resulting excitation energy is practically insensitive to the details of the nuclear ground state density profile.

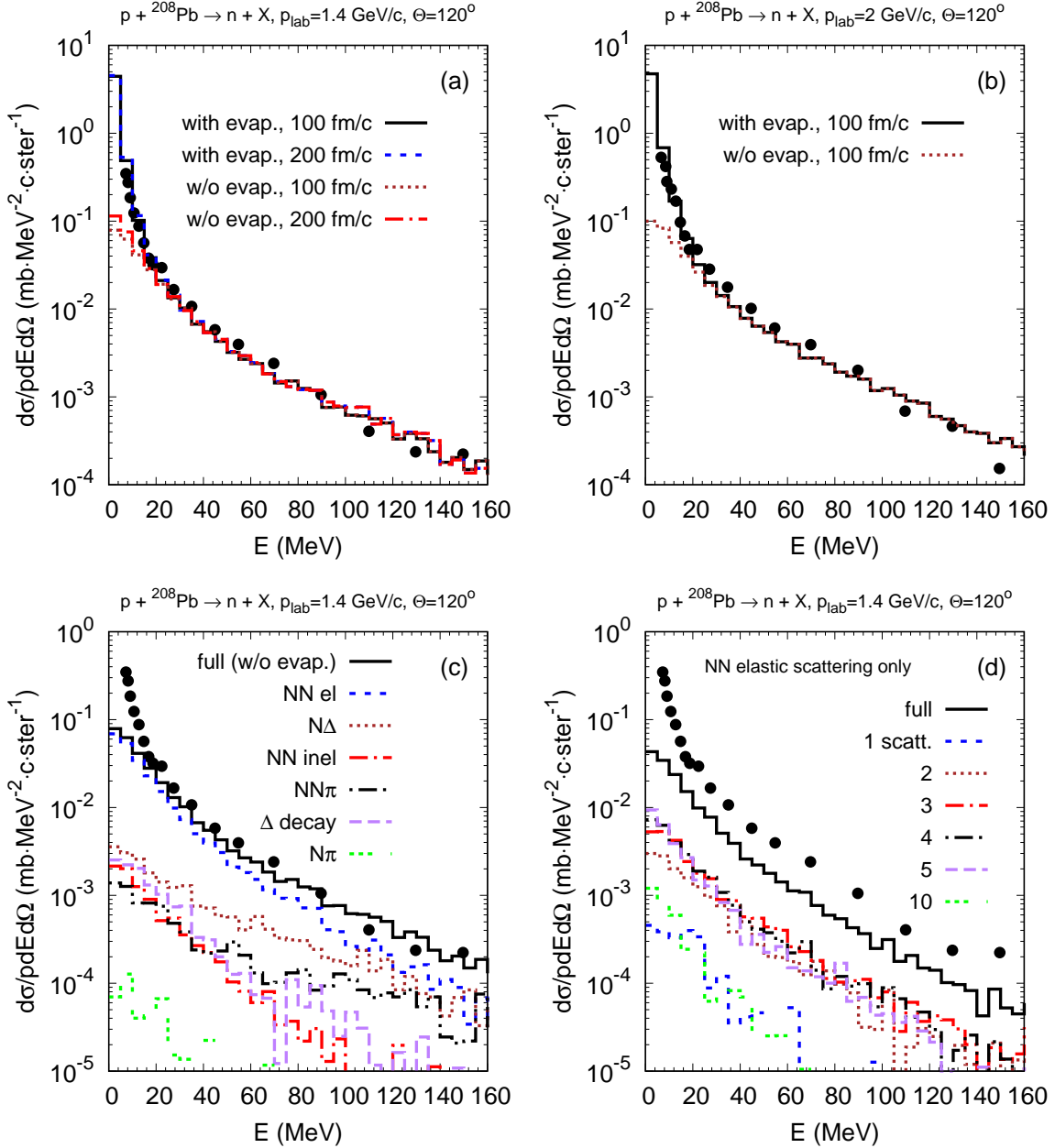


FIG. 1. Energy differential cross section of neutron production at  $\Theta = 120^\circ$  from  $p + {}^{208}\text{Pb}$  collisions at 1.4 GeV/c (a) and 2 GeV/c (b). The histograms show the calculations with and without inclusion of the neutron evaporation with the maximum time of the GiBUU calculation 100 and 200 fm/c as indicated. The panels (c),(d) display the calculation at 1.4 GeV/c stopped at 100 fm/c without evaporation (black solid histograms). (c): full GiBUU. The contributions of various neutron production channels are shown as indicated. (d): GiBUU with  $NN \rightarrow NN$  elastic scattering only. The contributions of the neutrons produced in a chain of the indicated number of scatterings are shown. Experimental data are from [26].

nuclear surface at the impact parameters  $b = 0.5, 1.0, \dots, 7$  fm with 2000 events for every impact parameter. (In calculating the spectrum the events were weighted with impact parameter.) The GiBUU calculation was run until 100 and 200 fm/c and then the target residues were identified and used as the input to SMM calculation. The latter was run 10 times for every GiBUU event. The evaporated neutrons were then included in the total spectrum of emitted neutrons. As we see the evaporation substantially increases the yield of the low-energy ( $E \lesssim 30$  MeV) neutrons and explains the evident two-slope structure of the experimental neutron spectra. This is not surprising since the same data were explained earlier with similar approaches in ref. [13] and recently in [27].

Fig. 1c shows the neutron energy spectrum from 1.4 GeV/c  $p+^{208}\text{Pb}$  collisions with partial contributions of the  $NN$  elastic and inelastic collisions,  $N\Delta$  collisions,  $NN\pi$  (pion absorption by nucleon pair) and  $N\pi$  collisions, and  $\Delta$  resonance decays. We see that the main contribution to the spectrum of preequilibrium neutrons is given by  $NN$  elastic collisions. The  $N\Delta$  and  $NN\pi$  collisions make comparable in the magnitude contribution above 100 MeV neutron energy. Other neutron production channels are less important. (Note that the production channel is not changed by subsequent elastic rescatterings, e.g. neutrons produced in a  $p\Delta^- \rightarrow nn$  collision may rescatter elastically on the other nucleons, but they are still regarded as produced in the  $N\Delta$  collision.) By performing an additional calculation keeping only elastic scatterings we have established that the main contribution to the neutron spectrum comes from multiple scattering (from two- to five-step) processes as displayed in Fig. 1d. This suggests that the residual nuclear system is approaching thermally equilibrated state while dynamically emitting neutrons. This is a type of the situation where it is natural to apply the SMM model.

### 3.2. Muon-induced DIS on nuclei

In this section we analyze the E665 data on slow neutron production in inclusive  $\mu^- + ^{208}\text{Pb}$  and  $\mu^- + ^{40}\text{Ca}$  DIS processes at the beam energy of 470 GeV [9]. The scattered muon was sampled as described in sec. 2 with cuts  $\nu > 20$  GeV,  $Q^2 > 0.8$  GeV<sup>2</sup>. In the studied kinematics, a rather modest, on the scale of 20%, nuclear shadowing dominated by the resolved photon interactions with two nucleons is present for  $R_A = \sigma(\mu\text{Pb})/A\sigma(\mu\text{N})$ . In the setup of the E665 experiment, both inelastic and diffractive events were included. Applying

Abramovsky-Gribov-Kancheli cutting rules [28] we observe that the events where projectile interacted with two nucleons and diffractive events contribute equal cross sections to the final state. While in the diffractive events no neutrons are produced, in the interactions where two nucleons are wounded roughly twice as many neutrons are produced. Overall, this results in the disappearance of shadowing for inclusive cross section (similar to the cancellation for central rapidities in ref. [28]) and in the enhancement of the average number of wounded nucleons per event:

$$n_{\text{wound}} = 1/R_A \sim 1.25, \quad (14)$$

(see e.g. ref. [29]) increasing the average neutron multiplicity by roughly the same factor.

This implies that the constraints on the secondary interactions are somewhat stronger than those which we find in our analysis. For now we will neglect this effect.

Fig. 2 displays the mass number distribution (a), excitation energy distribution (b) and the correlation between the excitation energy and the mass number (c) of the residual nucleus for the  $^{208}\text{Pb}$  target. Calculations in all models produce a sharp peak in the mass number distribution for the removal of only one nucleon and the broad tail towards larger mass number loss. For example, in the calculation with  $p_{\text{cut}} = 1 \text{ GeV}/c$ , 48% of residual nuclei have  $A_{\text{res}} = 207$ , while in the QDM calculation – 13%. In such events, a hole is produced due to initial hard DIS and the produced particles do not interact with the residue. Thus, the calculation with the strongest restriction on the momentum of an interacting particle produces the largest fraction of one-hole events. The excitation energy distributions have a two-slope structure with a kink at  $E_{\text{res}}^* = 50 - 70 \text{ MeV}$ . The region  $E_{\text{res}}^* < E_F \simeq 37 \text{ MeV}$  is saturated by one-hole excitations mostly. Higher excitation energies are only possible for the multiple (2,3,...) hole excitations. The dependence of the excitation energy on the number of removed nucleons is close to linear,  $\langle E_{\text{res}}^* \rangle \simeq 10 \text{ MeV}(A - A_{\text{res}})$ . Due to the Fermi motion, however, the distribution in the excitation energy for fixed number of removed nucleons is quite broad. We checked that this distribution practically does not depend on the treatment of the pattern of the hadron formation in calculations.

The spectrum of emitted neutrons is shown in Fig. 3. Below 1 MeV, the spectrum is almost entirely due to a statistical evaporation from an excited nuclear residue. In this low energy region the number of neutrons depends weakly on the excitation energy of the nuclear residue (and thus on the treatment of hadron formation), since with decreasing  $E_{\text{res}}^*$  the energy spectrum of evaporated neutrons becomes more steep. The sensitivity of

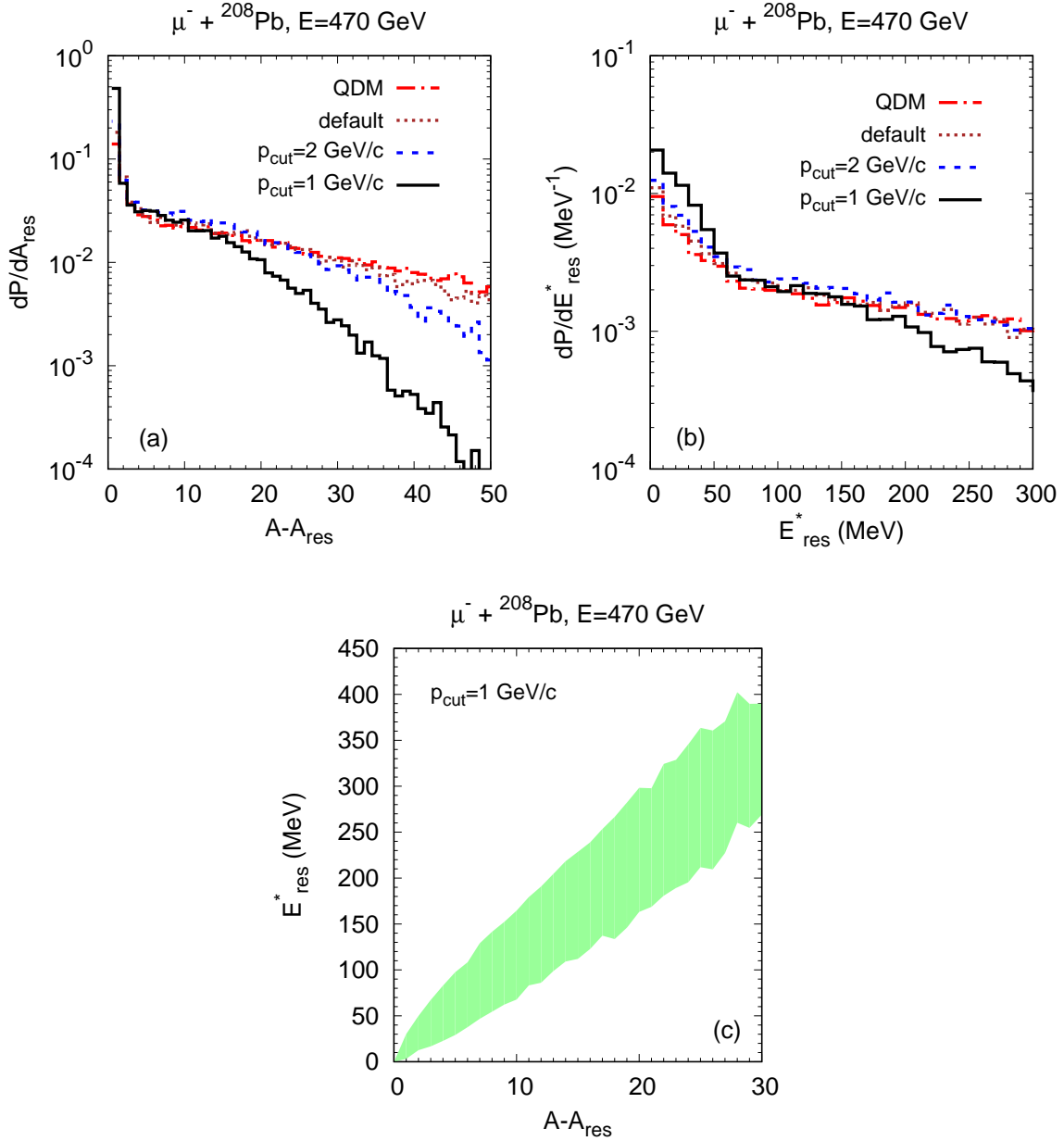


FIG. 2. Characteristics of the residual nucleus in  $\mu^- + {}^{208}\text{Pb}$  DIS at 470 GeV. On panels (a) and (b), different histograms correspond to different prescriptions for the hadron formation as indicated. (a) Probability distribution of the mass number loss  $A - A_{\text{res}}$ . (b) Probability distribution of the excitation energy. (c) Excitation energy as a function of the mass number loss obtained in GiBUU calculation with cutoff momentum  $p_{\text{cut}} = 1$  GeV/c. The upper (low) boundaries of the band correspond to the average value  $\langle E^* \rangle$  plus (minus) standard deviation.

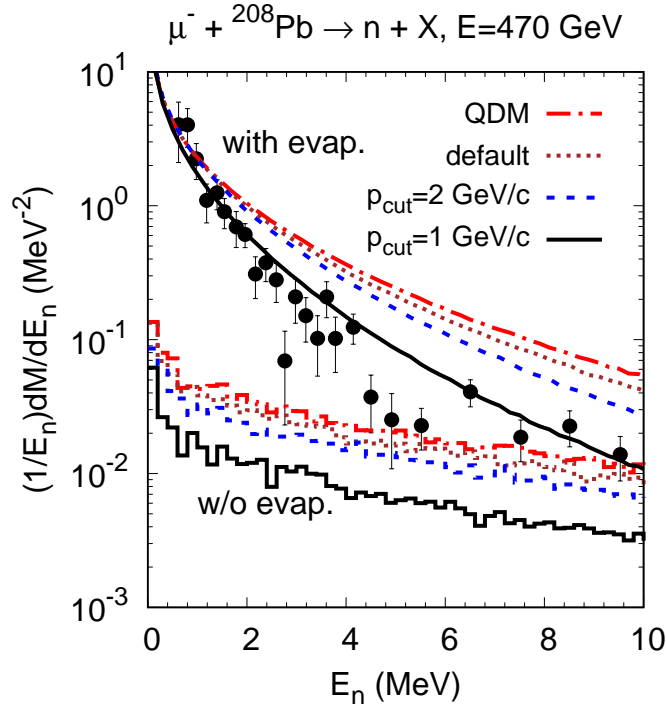


FIG. 3. Energy spectrum of emitted neutrons in  $\mu^- + {}^{208}\text{Pb}$  DIS at 470 GeV. The different types of lines and histograms correspond to the different treatments of hadron formation as indicated. Lines (histograms) are calculated with (without) adding evaporated neutrons from the nuclear residue. Experimental data are from ref. [9].

the spectrum to various treatments of hadron formation increases with neutron energy. The QDM and default calculations overestimate the neutron yields. Only a very strong restriction on the momentum of the particles which are allowed to interact ( $p < p_{\text{cut}} = 1$  GeV/c) describes the E665 data.

We have also performed calculation by setting  $p_{\text{cut}}$  to a very large value (1 TeV) which can be considered as no formation at all. It turned out that this calculation produces almost indistinguishable with QDM yields of neutrons below 10 MeV (of course, at higher neutron energies the QDM calculation gives smaller yields than the calculation with instantly formed hadrons). However, the default GiBUU calculation gives smaller yields of slow neutrons than QDM. It appears that the difference originates mainly from much larger expansion time (i.e. the string proper time between the hard interaction and first string breaking space-time points) in the GiBUU model [22]. In other words, the effective cross section of Eq.(8) is set

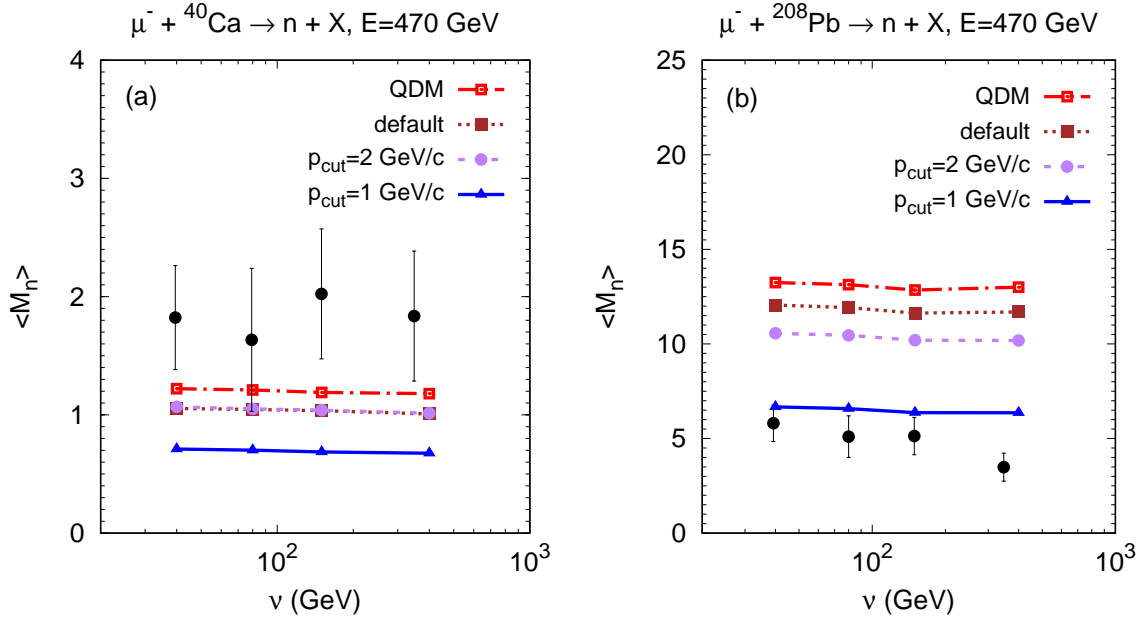


FIG. 4. Multiplicity of neutrons with energy  $E_n < 10$  MeV as a function of a virtual photon energy for (a)  $\mu^- + {}^{40}\text{Ca}$  and (b)  $\mu^- + {}^{208}\text{Pb}$  DIS at 470 GeV. Experimental data are from ref. [9].

to zero for  $t < t_{\text{prod}}$  in GiBUU. Having successfully described the E665 data for the lead target with  $p_{\text{cut}} = 1$  GeV/c we would expect that the description of the data for a lighter target nucleus will require even a lower value of the cutoff momentum. This is because a hadron will not interact with the target nucleus if its formation length is comparable with the nuclear size. Thus, from Eq.(2), we conclude that the cutoff momentum should be proportional to the nuclear radius. This clear picture is, however, not supported by the experimental data. Fig. 4 shows the average neutron multiplicity vs the photon energy  $\nu$  for the calcium and lead targets. In the case of  ${}^{40}\text{Ca}$  target the neutron multiplicities are underestimated by a factor of 2.5 in the calculation with  $p_{\text{cut}} = 1$  GeV/c and by 30% – in the QDM calculation. Thus, we fail to describe the E665 data for the calcium target based on the present-day formation length concept.

### 3.3. Quasireal photon interactions with nuclei at the LHC and RHIC

It is widely realized now that it is feasible to study the UPCs of heavy ions at colliders. In such processes, one of the ions serves as a source of the quasireal photons which interact with the second ion leaving the first ion intact, for a detailed discussion see ref. [30]. The

UPCs are now intensively studied at the LHC, for a summary of the recent results and references see ref. [31].

The maximum photon longitudinal momentum can be estimated in the c.m. frame of colliding nuclei (collider laboratory frame) from the condition that the photon wave length is equal to the radius of the Lorentz-contracted emitting nucleus [30], i.e.  $k_L^{\max} \simeq \gamma_L/R_A$ , where  $\gamma_L$  is the Lorentz factor. Assuming symmetric colliding system, we get  $k^{\max} = \gamma_L 2k_L^{\max} \simeq 2\gamma_L^2/R_A$  in the rest frame of another colliding nucleus. The estimated values of the maximum photon momentum  $k^{\max}$  and of the  $\gamma^*N$  c.m. energy  $W$  are listed in Table I (see also Table 1 in ref. [30])

TABLE I. Parameters of UPCs Au+Au at RHIC and Pb+Pb at LHC.

	$\sqrt{s_{NN}}$ (TeV)	$\gamma_L$	$k^{\max}$ (TeV/c)	$W$ (GeV)
RHIC	0.2	106	0.642	34.7
LHC	5.5	2931	477	946

In this paper, we will consider the simplest case when the photon experiences a hard interaction with one nucleon only. This condition is satisfied for the interaction of a direct photon with  $x_g \geq 0.01$  gluon leading to the production of the two high- $p_t$  jets. (The choice of  $x_g$ -range is dictated by the requirement that the gluon shadowing is small for the  $p_t$ -range of jets currently used in the experimental analysis:  $|p_t(\text{jet}_1)| + |p_t(\text{jet}_2)| \geq 40$  GeV.) Since under these conditions the nucleon fragmentation is practically not known experimentally, we use the PYTHIA model in which the fragmentation of nucleon weakly depends on  $x$  for moderate  $x$  and on the type of the removed parton. In principle, due to the color effects, the cases of the removal of a gluon (which is our main interest) and a quark from the nucleus may differ. In particular, in the Lund model, the removal of a gluon,  $\gamma g \rightarrow 2\text{jets}$ , corresponds to the attachment of two strings to a nucleon leading to somewhat softer jets as compared to the quark case,  $\gamma q \rightarrow q'$ . (This effect would be possible to test in  $pA$  UPCs.) For now we neglect this difference and rely on the inclusive set of the PYTHIA events under certain kinematic conditions.

Since the PYTHIA model describes a  $\gamma^*$ -nucleon collision with the photon emitted by the scattered lepton, it is impossible to initialize an exactly real photon. However, by varying

the kinematics of the lepton scattering one can change the photon virtuality  $Q^2$  (or Bjorken  $x = Q^2/2\nu m_N$ ) and the relative flux of the longitudinal photons  $\epsilon$ . We have checked that the variation of  $\epsilon$  in the interval  $0.02 - 0.10$  has practically no effect on the results. In the calculations below we set  $\epsilon = 0.05$ . The  $z$ -axis is directed along the photon momentum.

As representative values of the  $\gamma^*N$  c.m. energy at the LHC we have chosen  $W = 100$  GeV and  $W = 500$  GeV. The Bjorken  $x$  has been set to  $M_{\text{dijet}}^{(0)2}/W^2$  with  $M_{\text{dijet}}^{(0)} = 40$  GeV which gives  $x = 0.16$  for  $W = 100$  GeV and  $x = 6.4 \cdot 10^{-3}$  for  $W = 500$  GeV. This is equivalent to modeling the dijet production with invariant mass  $M_{\text{dijet}} > M_{\text{dijet}}^{(0)}$  by the direct photon on a gluon with  $x_g = M_{\text{dijet}}^2/W^2$ . The lower boundary imposed on  $x_g$  guaranties the smallness of the shadowing effects.

We have also performed calculations at RHIC kinematics with  $W = 30$  GeV,  $x = 0.16$ . This corresponds to setting the threshold dijet invariant mass  $M_{\text{dijet}}^{(0)} = 12$  GeV.

We checked that the mass and excitation energy distributions of residual nuclei and the correlation between  $E_{\text{res}}^*$  and  $A$  in the LHC kinematics are almost identical to those for E665 kinematics shown in Fig. 2. (Thus, the respective plots for the LHC are not shown.) The shape of neutron multiplicity distributions shown in Fig. 5(a) for LHC kinematics reflects the shape of the excitation energy distributions of the nuclear residues (Fig. 2b) with a broad maximum near  $E_{\text{res}}^* = 0$  and a long tail of high energy excitations. The variation of the photon kinematics and of the target nucleus has only a little effect on the neutron multiplicity distribution as demonstrated in Fig. 5(b) for  $p_{\text{cut}} = 1$  GeV/c. This holds true also for other prescriptions for the hadron formation (not shown). Some excess of events with low neutron multiplicities is visible in the case of  $^{197}\text{Au}$  target with smaller  $N/Z$  ratio.

Fig. 6(a) shows the neutron low- $p_t$  spectra for different prescriptions for hadron formation. At very small transverse momenta, statistical emission reduces the effect of hadron formation. However, already above  $p_t \simeq 100$  MeV/c we observe a much stronger dependence of the neutron emission on the pattern of hadron formation. Observing this effect would require a highly segmented zero degree calorimeter (ZDC). As shown in Fig. 6(c), the spectra at low  $p_t$ 's are almost independent on  $W$ ,  $x$  and on the choice of the nuclear target. This means that the convolution with the photon flux should not influence the low- $p_t$  spectra of neutrons.

In contrast, the high- $p_t$  neutron spectra do not depend on the prescription for hadron formation (Fig. 6(b)). But the dependence on photon kinematics becomes evident at high

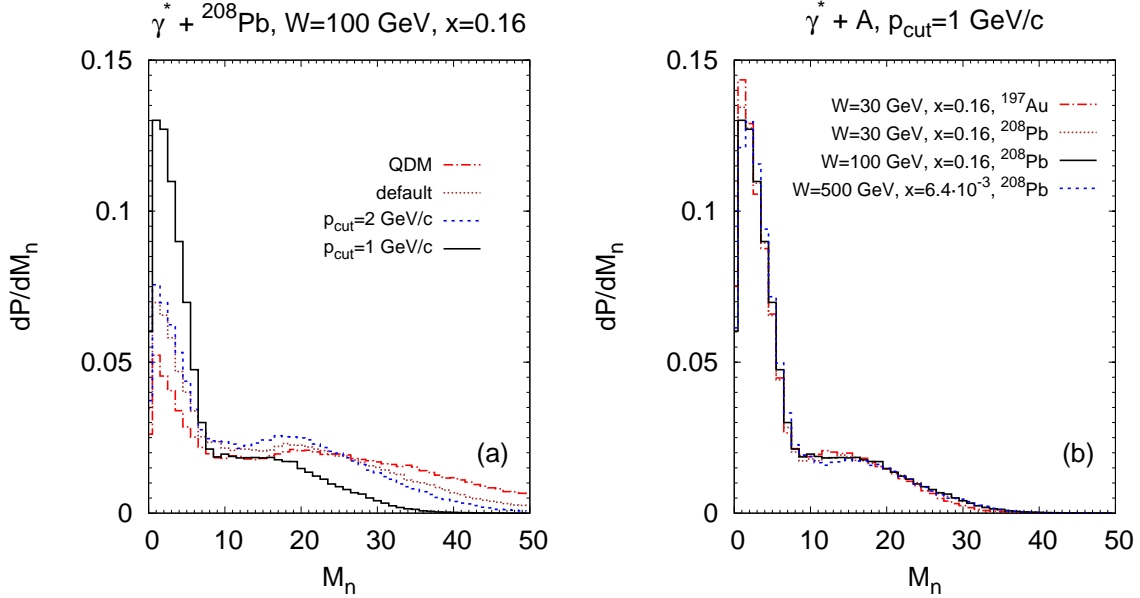


FIG. 5. Neutron multiplicity distributions for  $\gamma^* + \text{nucleus}$  deep inelastic collisions. Panel (a) shows the results with fixed photon kinematics  $W = 100$  GeV,  $x = 0.16$  on the  ${}^{208}\text{Pb}$  target for different prescriptions for hadron formation as indicated. The average neutron multiplicities (standard deviations) are: 17.9(14.3) for QDM, 15.2(12.6) for default, 13.7(11.3) for  $p_{\text{cut}} = 2$  GeV/c, and 7.7(8.0) for  $p_{\text{cut}} = 1$  GeV/c. Panel (b) compares the results calculated with  $p_{\text{cut}} = 1$  GeV/c for the different photon kinematics and nuclear targets as indicated.

neutron transverse momenta (Fig. 6(d)). Since most high- $p_t$  neutrons are produced in the hard DIS process directly, the neutron yields for different  $x$  and  $W$  at fixed  $p_t$  can be explained by the growing gluon distribution function with decreasing  $x_g = x + 4p_t^2/W^2$  and almost coincide with the neutron yields from the elementary  $\gamma^* + p$  collisions at the corresponding  $x$  and  $W$  (Fig. 7).

The sensitivity of the low-transverse-momentum neutron yield to hadron formation implies that a large part of such neutrons is produced in secondary interactions (the interactions of slow neutrons themselves are not influenced by hadron formation). To better understand the sources of slow neutrons, let us again consider the elementary  $\gamma^* + p$  deep inelastic collisions in the same kinematics. Fig. 8 shows the inclusive  $x_F$ - and momentum-distributions of pions, protons, and neutrons. The Feynman variable  $x_F$  is defined as

$$x_F = \frac{E - p^z}{m_N}, \quad (15)$$

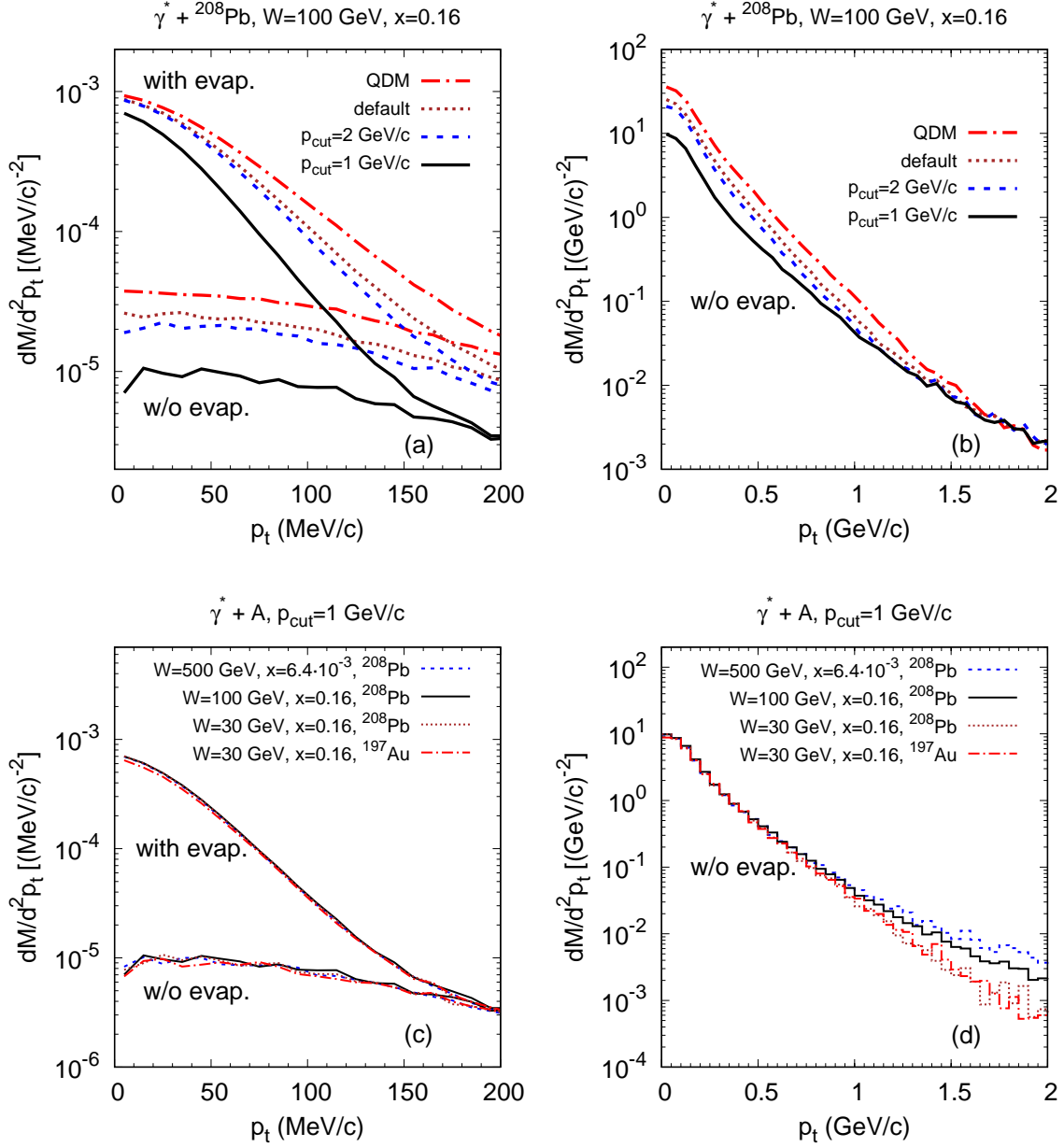


FIG. 6. Neutron transverse momentum spectra for  $\gamma^*$ +nucleus deep inelastic collisions. (a) Spectra for fixed photon kinematics  $W = 100$  GeV,  $x = 0.16$  on the  ${}^{208}\text{Pb}$  target with different prescriptions for hadron formation as indicated. Upper (lower) lines show calculations with (without) statistical evaporation. (b) Same as (a) without evaporation, but for the large range of neutron transverse momentum. (c) Spectra for the different photon kinematics and nuclear targets as indicated calculated with  $p_{\text{cut}} = 1$  GeV/c. (d) Same as (c) without evaporation, but for the large range of neutron transverse momentum.

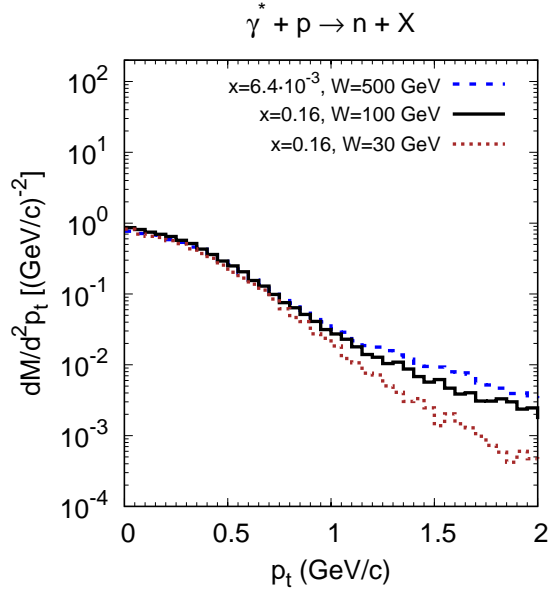


FIG. 7. Neutron transverse momentum spectra for  $\gamma^* + p$  deep inelastic collisions for the different photon kinematics as indicated.

where  $E$  and  $p^z$  are the particle energy and the longitudinal component of momentum in the target rest frame, respectively. The condition  $x_F < 1 - x$  is fulfilled, as follows from target fragmentation. Overall this leads to the enhancement of the slow particle production with decreasing  $x$ , which is best noticeable for protons (Fig. 8(c),(d)).

The directly produced slow neutrons are even more sensitive to the photon kinematics (Fig. 8(e),(f)). Like in the proton case, the neutron spectrum also shifts to smaller momenta with decreasing  $x$ , but in addition gets significantly suppressed because the  $p \rightarrow n$  transition involves the valence quark.

We see that pions (Fig. 8(a),(b)) are most abundant. The yields of protons and neutrons are suppressed by an order of magnitude relative to the pion yield. Thus, pions govern the secondary particle interactions in the target nuclei. The pion  $x_F$ -spectra for different  $W$  and same  $x$  almost coincide. The dependence on Bjorken  $x$  is visible only close to the upper limit of  $x_F$ . Also the momentum spectra of pions are largely independent on  $W$  and  $x$ . This leads to the independence of the secondary slow neutron production in photon-nucleus reactions on  $W$  and  $x$ .

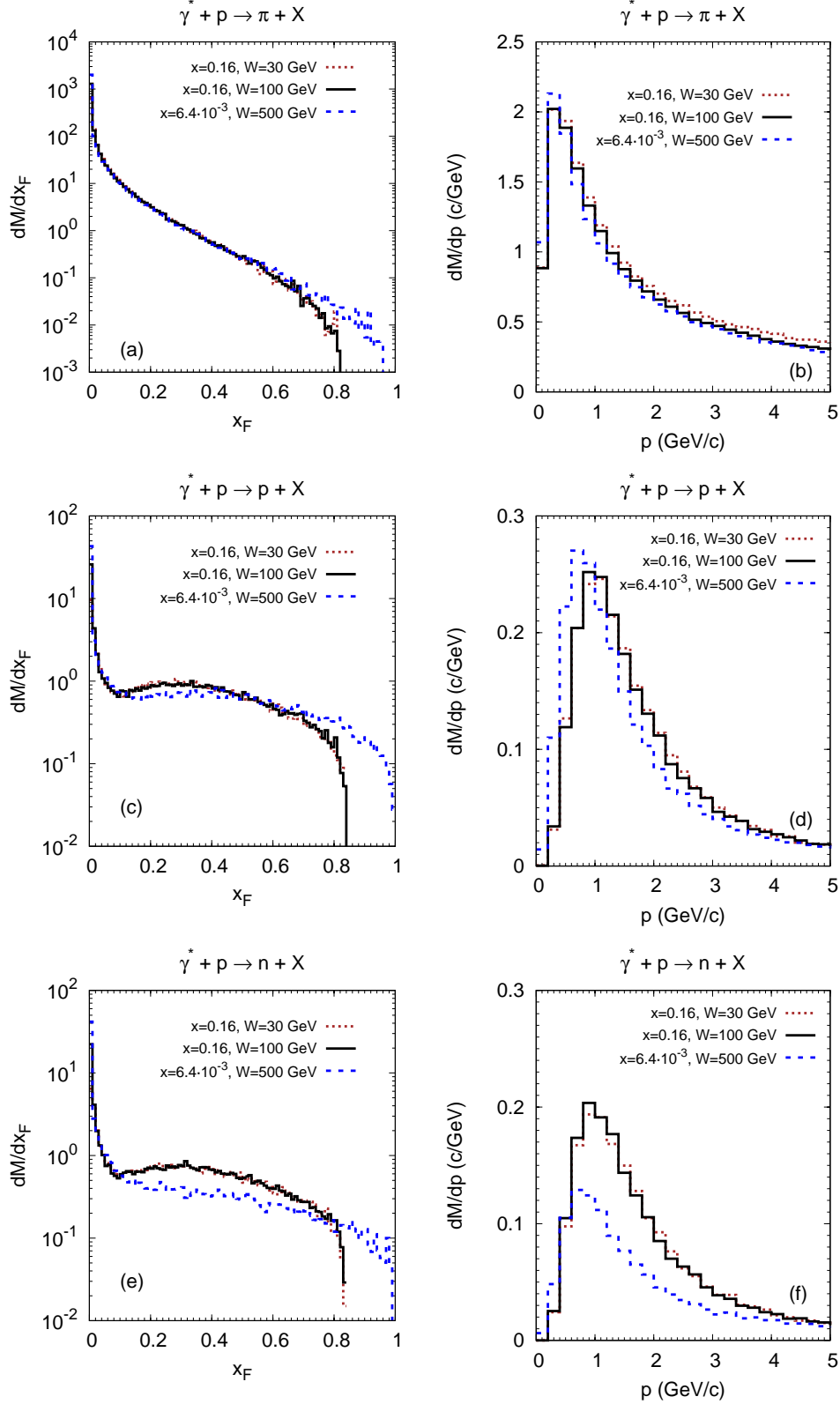


FIG. 8.  $x_F$ - and momentum-spectra of pions [panels (a),(b), respectively], protons [(c),(d)], and neutrons [(e),(f)] produced in  $\gamma^* + p$  collisions at the indicated kinematics. The spectra are normalized to the number of respective particles per deep inelastic event.

#### 4. DIRECTIONS FOR FURTHER STUDIES

We have considered the elementary process most close to the leading twist DIS – production dijets in the direct photon gluon interaction in the kinematics where nuclear shadowing effects are small. Here we outline several other interesting processes.

(a) In the model we ignored possible differences between the final state interactions for the case of the gluon and quark removals. One possible difference arises in the Lund string model where effectively two strings are approximating an octet residual system. Other effect is a larger energy loss in the propagation of a color octet dijet through the media leading to a higher nuclear excitation energies due to larger number of wounded nucleons.

(b) Production of dijets in the resolved photon - nucleus collision when dijet carries the light cone fraction of the photon momentum,  $x_\gamma$  substantially smaller than one. The selection of a parton with smaller  $x_\gamma$  in the photon corresponds to selection of configurations with a larger number of partons. For  $x_\gamma \lesssim 0.1$ , these configurations should interact with the target with the strength comparable to the strength of interaction of configurations responsible for nuclear shadowing in coherent diffraction photoproduction of  $\rho$ -mesons off nuclei [32]. Based on this analysis we expect that the average number of wounded nucleons should be  $n_{\text{wound}} \sim 3$ . Correspondingly, the average number of emitted neutrons should increase by a factor of 3 since the fragmentation of each of the wounded nucleons is independent to a first approximation.

(c) One can consider generic  $\gamma A$  collisions. Based on the analysis [33] of the color fluctuations in photon we expect that in these collisions the average number of wounded nucleons would be large and fluctuating strongly. The number of emitted neutrons should be correlated with  $p_t$  of the leading particles produced in the photon fragmentation region (smaller  $p_t$  – larger neutron number).

(d) It appears feasible to detect charm particles in the UPCs. At large  $W \geq 100$  GeV and small enough  $p_t \lesssim \text{few GeV}$ , one reaches the kinematics where the nuclear shadowing becomes significant (a factor of two reduction of the cross section as compared to the impulse approximation) resulting in wounding in average two nucleons and hence increasing the number of neutrons by a factor of two.

## 5. SUMMARY AND CONCLUSIONS

We have performed the hybrid, i.e. dynamical plus statistical, calculations of the slow neutron production in proton- and hard-virtual-photon-induced inelastic collisions with nuclei. For the dynamical stage, the GiBUU model [14] has been applied. The statistical stage has been described within the SMM model [15, 16]. For the calculation of characteristics  $(A_{\text{res}}, Z_{\text{res}}, E_{\text{res}}^*, \mathbf{p}_{\text{res}})$  of a nuclear residue, the procedure based on the hole excitations in Fermi sea has been developed. We have tested the hybrid calculations by comparison with available data on neutron production in proton- and muon-nucleus interactions.

The multiplicity of slow ( $E < 10$  MeV) neutrons in  $\mu^-$  DIS on Pb measured by E665 collaboration [9] is a factor of two smaller than what is expected from GiBUU+SMM calculations both with default treatment of hadron formation (based on hadron production and formation space-time points from JETSET) and with the quantum diffusion model of CT. The only scenario which allows to reproduce the neutron multiplicity and the energy spectrum in  $\mu^- + {}^{208}\text{Pb}$  DIS is the one in which only produced hadrons with momenta below 1 GeV/c are allowed to interact with the rest of the nucleus. If we translate this momentum cutoff to the formation length, we would get the mass denominator  $\Delta M^2 \sim p_{\text{cut}}/R \sim 0.03$  GeV<sup>2</sup> in Eq.(2), where  $R = 7$  fm is the radius of the lead nucleus. This value of  $\Delta M^2$  is an order of magnitude smaller than the baseline value extracted from pion exclusive electroproduction at TJNAF. The use of the 1 GeV/c cutoff unfortunately leads to the underestimation of the E665 data on the multiplicity of slow neutrons in  $\mu^-$  DIS off Ca by 50%. Moreover, even the largest neutron multiplicities reached within the QDM are 30% below the E665 data for the calcium target.

All together this indicates the presence of a novel dynamics in the production of hadrons in the nucleus fragmentation region which cannot be reproduced by adjusting parameters of existing models. In hindsight this may be not too surprising as we are dealing with particles produced in the target fragmentation region while the models were designed to describe the space-time picture of hadron formation in the current fragmentation region. Hence, further studies are necessary to get a better understanding of the hadron formation in the target fragmentation region. In long run such studies would be possible to perform at the Electron-Ion Collider by measuring the  $A$ -dependence of hadron spectra in the nucleus fragmentation region.

However, already in the near future the study of hard  $\gamma A$  UPCs at the LHC and RHIC with detection of neutrons in the ZDC would allow to clarify the space-time picture of hadron formation in the nucleus fragmentation region. To this end we performed the exploratory studies of  $\gamma + \text{Pb(Au)}$  interactions in the direct photon regime in the LHC (RHIC) kinematics. We revealed a strong dependence of the neutron multiplicities and  $p_t$ -spectra on the model of hadron formation indicating that the slow neutron production provides an important window for studying the space-time picture of formation of slow hadrons in hard processes. We also listed several directions for further studies of the interplay of hard and soft dynamics in the UPC interactions.

## ACKNOWLEDGMENTS

The support by the Frankfurt Center for Scientific Computing is gratefully acknowledged. We thank Marcus Bleicher, Alexander Botvina and Leonid Frankfurt for stimulating discussions. We also thank Kai Gallmeister for constructive criticism concerning the implementation of nuclear residue determination procedure in GiBUU. We thank A. Angerami for discussion of the feasibility of the studies discussed in this paper and Yu. Dokshitzer for discussion of various mechanisms of the final state interactions. AL is grateful to the Department of Physics at the Pennsylvania State University, where this work was started, for the hospitality and financial support. AL also acknowledges partial financial support of HIC for FAIR within the framework of the Hessian LOEWE program. The research of MS was supported by the U.S. Department of Energy, Office of Science, Office of Nuclear Physics, under Award No. DE-FG02-93ER40771.

- 
- [1] L. L. Frankfurt, G. A. Miller, and M. Strikman, *Ann. Rev. Nucl. Part. Sci.* **44**, 501 (1994).
  - [2] P. Jain, B. Pire, and J. P. Ralston, *Phys. Rept.* **271**, 67 (1996).
  - [3] D. Dutta, K. Hafidi, and M. Strikman, *Prog.Part.Nucl.Phys.* **69**, 1 (2013).
  - [4] E. Aitala *et al.* (E791 Collaboration), *Phys.Rev.Lett.* **86**, 4773 (2001).
  - [5] M. D. Sokoloff *et al.*, *Phys. Rev. Lett.* **57**, 3003 (1986).
  - [6] M. R. Adams *et al.* (E665), *Phys. Rev. Lett.* **74**, 1525 (1995).
  - [7] S. Chekanov *et al.* (ZEUS Collaboration), *Nucl.Phys.* **B695**, 3 (2004).

- [8] S. Chekanov *et al.* (ZEUS Collaboration), *PMC Phys.* **A1**, 6 (2007).
- [9] M. R. Adams *et al.* (E665), *Phys. Rev. Lett.* **74**, 5198 (1995), [Erratum: *Phys. Rev. Lett.*80,2020(1998)].
- [10] K. Gallmeister and U. Mosel, *Nucl. Phys.* **A801**, 68 (2008), arXiv:nucl-th/0701064 [nucl-th].
- [11] A. Larson, G. A. Miller, and M. Strikman, *Phys. Rev.* **C74**, 018201 (2006).
- [12] A. B. Larionov, M. Strikman, and M. Bleicher, *Phys. Rev.* **C93**, 034618 (2016), arXiv:1601.00189 [nucl-th].
- [13] M. Strikman, M. G. Tverskoy, and M. B. Zhalov, *Phys. Lett.* **B459**, 37 (1999), arXiv:nucl-th/9806099 [nucl-th].
- [14] O. Buss, T. Gaitanos, K. Gallmeister, H. van Hees, M. Kaskulov, O. Lalakulich, A. B. Larionov, T. Leitner, J. Weil, and U. Mosel, *Phys. Rept.* **512**, 1 (2012), arXiv:1106.1344 [hep-ph].
- [15] A. S. Botvina, A. S. Iljinov, I. N. Mishustin, J. P. Bondorf, R. Donangelo, and K. Sneppen, *Nucl. Phys.* **A475**, 663 (1987).
- [16] J. P. Bondorf, A. S. Botvina, A. S. Ilinov, I. N. Mishustin, and K. Sneppen, *Phys. Rept.* **257**, 133 (1995).
- [17] G. A. Lalazissis, J. König, and P. Ring, *Phys. Rev.* **C55**, 540 (1997).
- [18] T. Sjostrand, S. Mrenna, and P. Z. Skands, *JHEP* **05**, 026 (2006), arXiv:hep-ph/0603175 [hep-ph].
- [19] B. Andersson, G. Gustafson, and H. Pi, *Z. Phys.* **C57**, 485 (1993).
- [20] H. Lenske, private communication.
- [21] M. E. Christy and P. E. Bosted, *Phys. Rev.* **C81**, 055213 (2010), arXiv:0712.3731 [hep-ph].
- [22] K. Gallmeister and T. Falter, *Phys. Lett.* **B630**, 40 (2005), arXiv:nucl-th/0502015 [nucl-th].
- [23] G. Farrar, H. Liu, L. Frankfurt, and M. Strikman, *Phys. Rev. Lett.* **61**, 686 (1988).
- [24] T. Gaitanos, A. B. Larionov, H. Lenske, and U. Mosel, *Phys. Rev.* **C81**, 054316 (2010), arXiv:1003.4863 [nucl-th].
- [25] V. Weisskopf, *Phys. Rev.* **52**, 295 (1937).
- [26] Yu. D. Bayukov *et al.*, ITEP-172-1983 (1983).
- [27] A. S. Galoyan, A. Ribon, and V. V. Uzhinsky, *JETP Lett.* **102**, 324 (2015), [*Pisma Zh. Eksp. Teor. Fiz.*102,no.6,361(2015)].
- [28] V. A. Abramovsky, V. N. Gribov, and O. V. Kancheli, *Yad. Fiz.* **18**, 595 (1973), [*Sov. J. Nucl. Phys.*18,308(1974)].

- [29] L. Bertocchi and D. Treleani, *J. Phys.* **G3**, 147 (1977).
- [30] A. J. Baltz, *Phys. Rept.* **458**, 1 (2008), arXiv:0706.3356 [nucl-ex].
- [31] A. Angerami (ATLAS Collaboration), Talk at QM 2018, ATL-PHYS-SLIDE-2018-270 (2018).
- [32] L. Frankfurt, V. Guzey, M. Strikman, and M. Zhalov, *Phys. Lett.* **B752**, 51 (2016), arXiv:1506.07150 [hep-ph].
- [33] M. Alvioli, L. Frankfurt, V. Guzey, M. Strikman, and M. Zhalov, *Phys. Lett.* **B767**, 450 (2017), arXiv:1605.06606 [hep-ph].